



Published in final edited form as:

Nat Nanotechnol. 2014 June ; 9(6): 481–487. doi:10.1038/nnano.2014.62.

## Selective uptake of single walled carbon nanotubes by circulating monocytes for enhanced tumour delivery

Bryan Ronain Smith<sup>1,2</sup>, Eliver Eid Bou Ghosn<sup>3</sup>, Harikrishna Rallapalli<sup>1</sup>, Jennifer A. Prescher<sup>1,4</sup>, Timothy Larson<sup>1,2</sup>, Leonore A. Herzenberg<sup>3</sup>, and Sanjiv Sam Gambhir<sup>1,2,5</sup>

<sup>1</sup>Molecular Imaging Program at Stanford, Stanford University, Stanford, CA, 94305

<sup>2</sup>Department of Radiology, Stanford University, Stanford, CA, 94305

<sup>3</sup>Department of Genetics, Stanford University, Stanford, CA, 94305

<sup>5</sup>Department of Bioengineering, Department of Materials Science & Engineering, Stanford University, Stanford, CA, 94305

### Abstract

In cancer imaging, nanoparticle biodistribution is typically visualised in living subjects using ‘bulk’ imaging modalities such as magnetic resonance imaging, computerized tomography and whole-body fluorescence. As such the nanoparticle influx is observed only macroscopically and the mechanisms by which they target cancer remain elusive. Nanoparticles are assumed to accumulate via several targeting mechanisms, particularly extravasation ie, leakage into tumour. Here we show that, in addition to conventional nanoparticle uptake mechanisms, single-walled carbon nanotubes are almost exclusively taken up by a single immune cell subset, Ly-6C<sup>hi</sup> monocytes (almost 100% uptake in Ly-6C<sup>hi</sup> monocytes, below 3% in all other circulating cells), and delivered to the tumour in mice. Next, we demonstrate that a targeting ligand (RGD) conjugated to nanotubes significantly enhances the number of single-walled carbon nanotube-loaded monocytes reaching the tumour ( $p < 0.001$ , day 7 p.i.). The remarkable selectivity of this tumour targeting mechanism demonstrates an advanced immune-based delivery strategy for enhancing specific tumour delivery with substantial penetration.

---

The diagnostic and therapeutic efficacy of cancer-targeted nanoparticles in clinical applications is limited by a lack of understanding of their tumour targeting properties.

---

Users may view, print, copy, and download text and data-mine the content in such documents, for the purposes of academic research, subject always to the full Conditions of use:[http://www.nature.com/authors/editorial\\_policies/license.html#terms](http://www.nature.com/authors/editorial_policies/license.html#terms)

Corresponding Authors: Bryan R. Smith: [brsmith@stanford.edu](mailto:brsmith@stanford.edu); Sam Gambhir: [sgambhir@stanford.edu](mailto:sgambhir@stanford.edu), Departments of Radiology & Bioengineering, Clark center, East Wing, First Floor E150, 318 West Campus Drive, Stanford CA, 94305.

<sup>4</sup>Present address: Department of Chemistry, University of California, Irvine, Irvine, CA 92697.

### Contributions

B.R.S. and S.S.G. conceived and designed the experiments. B.R.S. performed the experiments and contributed materials and analysis tools. B.R.S. and S.S.G. analysed the data and wrote the paper. E.E.B.G. designed, performed, and analysed 12-colour, 14-parameter FACS for immune cell analysis of blood samples, discussed results, contributed reagents, and commented on the manuscript. L.A.H. assisted with guidance and analysis for high-dimensional flow cytometry and contributed materials/analysis tools. H.R. assisted with analyses of intravital imaging experiments. B.R.S. and J.A.P. designed, performed, and analysed initial flow cytometry assays. T.L. assisted with characterization of nanotubes.

Supplementary information accompanies this paper at [www.nature.com/naturenanotechnology](http://www.nature.com/naturenanotechnology).

Reprints and permission information is available online at <http://npg.nature.com/reprintsandpermissions/>.

Typically, nanoparticles are believed to target tumours via passive (e.g., blood vessel leakiness, such as in the enhanced permeability and retention (EPR) effect<sup>1, 2</sup>) and/or active (e.g., ligand-mediated<sup>2-4</sup>) targeting. With and without ligand-mediated targeting, single-walled carbon nanotubes (SWNTs) have been shown to display some of the highest tumour uptake values of all intravenously injected nanoparticles<sup>5</sup>. For this reason, we chose to examine SWNT targeting in detail.

Currently, most studies visualise nanoparticle localization using bulk imaging modalities such as MRI, ultrasound, and whole body fluorescence<sup>6</sup>. When nanoparticle signal is observed with such imaging modalities, it is typically presumed that well-known targeting mechanisms are the cause of nanoparticle accumulation. Here we ask whether nanoparticles may target tumour via other routes, and what are the consequences and advantages of such routes on the field of cancer nanotechnology.

Recently, we demonstrated that SWNTs can target tumour cells via both passive and active mechanisms in a mouse tumour model, including extravasation from the bloodstream into tumour interstitium (passive) and ligand-mediated targeting to tumour cells and to tumour blood vessels (active)<sup>7</sup>. However, we found that the uptake of SWNTs into tumours could not be explained by these mechanisms alone<sup>7</sup>. In this work, we identify and characterise the other mechanisms mediating the uptake of SWNTs into tumour by dynamic imaging on the microscale and determine if these other mechanisms are ligand-mediated in nature. Based on initial observations<sup>7</sup>, we hypothesised that cells in the blood take up nanoparticles and deposit them in the tumour, with increased uptake due to ligand targeting. Uncovering these alternative tumour uptake mechanisms could lead to new ways to increase efficient nanoparticle deposition in tumour, improved methods for tumour diagnosis or treatment and, potentially, to novel ways to influence an immune cell subset for cancer therapy and other applications.

## Circulating Blood Cells Rapidly Internalize SWNTs

To monitor SWNTs in living mice, we employed intravital microscopy (IVM)<sup>8</sup> with a dorsal skin fold chamber mouse tumour model<sup>7</sup> (Supplementary Fig. S1). Three days after dorsal window implantation, tumour cells were implanted under the window. Ten days later, SWNTs (plain or peptide-modified, all with fluorescent dye, Cy5.5; Fig. 1b) were injected via the tail vein. We observed the influx of SWNTs into blood vessels within seconds (see Supplementary Movie 1). Subsequently, we observed the appearance of discrete compartments of approximately the size and shape of cells in the SWNT (Cy5.5) fluorescent channel flowing through the blood vessels (Fig. 1a, Supplementary Movie 1).

We discovered that ~8  $\mu\text{m}$  circulating cells take up SWNTs using Fluorescence-Activated Cell Sorting (FACS) and dark-field fluorescence microscopy (see Fig. 1c-d and Supplementary Movie 2). We verified that SWNTs were taken up into the circulating blood cells (Fig. 1c), not simply Cy5.5 dye alone, by applying hyperspectral imaging to compare the spectral signatures of a plain SWNT (modified only with PEG and Cy5.5) solution to those of FACS-sorted SWNT-positive cells (Fig. 1c-d); a negative control of mice never injected with SWNTs showed no SWNT signal in the cells (Supplementary Fig. S2). The

hyperspectral analysis also provides a map of the subcellular spatial distribution of SWNTs. SWNTs appear dispersed throughout much of the cell cytoplasm and sparsely around the cell membrane (Fig. 1c). This suggests that SWNTs are predominantly taken up into the cells, rather than binding to the cell surface.

## Selective Uptake of SWNTs by Inflammatory Blood Monocytes

Intrigued by the SWNT uptake into cells, we sought to define the cell subsets. In some mice, submandibular bleeding was performed 2h and 6h post-injection (p.i.). We employed high-dimensional 14-parameter (12-colour) FACS analysis to identify the subset(s) of immune cells that takes up SWNTs in the blood. SWNTs reputedly can, and generally do, enter a wide variety of cells via energy-dependent and independent uptake mechanisms<sup>9, 10</sup>. Based on previous extensive studies, it was expected that phagocytes such as circulating macrophages and their precursors<sup>11–13</sup>, among other circulating cells, would take up SWNTs.

In contrast, we show that of all myeloid cells, only a single monocyte subset, Ly-6C<sup>hi</sup> monocytes, displayed substantial SWNT uptake; circulating Ly-6C<sup>hi</sup> monocytes took up SWNTs with exquisite selectivity (nearly 100% of Ly-6C<sup>hi</sup>, CD11b<sup>+</sup> monocytes) within 2h p.i. (Fig. 2). Other circulating white blood cells, including phagocytic cells, took up negligible amounts of SWNTs (e.g., ~3% of neutrophils, <1% of Ly-6C<sup>low</sup> monocytes, <1% of lymphocytes, etc.; Fig. 2). High selectivity for the Ly-6C<sup>hi</sup> subset was still observed at 6h p.i. in blood (Fig. 2), after freely-circulating SWNTs had already cleared from vasculature<sup>8</sup>. We do not yet understand the mechanisms (e.g., specific surface receptors) by which Ly-6C<sup>hi</sup> monocytes selectively recognize and internalize SWNTs. Nevertheless, intriguingly the uptake of SWNTs by Ly-6C<sup>hi</sup> monocytes does not activate these cells 6h after injection (Supplementary Fig. S3).

## SWNT Surface Functionalization Enhances Monocyte Uptake into Tumour

We observed that SWNT-laden monocytes entered tumour interstitium (Fig. 3a) under all conditions (with and without peptide). Intravital imaging observations demonstrated SWNT-loaded monocytes both rapidly flowing and interacting with vascular endothelium in the tumour (Supplementary Movie 3). We visualized SWNT-laden monocytes crawling along the surface of blood vessels with subsequent flattening along the vessel wall, as commonly observed in monocyte extravasation (Supplementary Movie 4), implicating the blood as the source of tumour-infiltrating monocytes. Next, we asked whether the presence of specific peptide on the SWNT surface affected monocyte homing to tumour. RGD is a peptide sequence commonly used as a ligand for nanoparticle targeting to bind to the integrin  $\alpha_v\beta_3$ , which is expressed on the surface of angiogenic tumour blood vessels (and some tumour cells)<sup>14, 15</sup>; RAD peptide serves as a non-specific control. Intriguingly, on day 1 p.i. we observed significantly more SWNT-laden monocytes in tumour interstitium in the RGD-SWNT injected group compared to the RAD-SWNT group ( $p=0.01$ , Fig. 3b). Interestingly, monocytes continued to home to tumour over time in mice that received RGD-SWNTs, with more SWNT-laden monocytes in the tumour interstitium in the RGD-SWNT condition than the RAD-SWNT condition on day 7 p.i. ( $p<0.0005$ , Fig. 3b); the difference between RGD

and RAD conditions was even greater on day 7 than on day 1 (Fig. 3b). The integrin-specific peptide on the SWNT surface thus surprisingly appears to help drive monocytes into tumour interstitium (previously, it was known only that RGD can assist free nanoparticle accumulation in tumour<sup>7, 14, 15</sup>); this is consistent with our analysis of monocyte interactions with the tumour vasculature in the RGD-SWNT group (see Supplementary Fig. S4 and Supplementary Information for discussion) and the trend of increasing total SWNT accumulation in tumour (Supplementary Fig. S5), suggesting the phenomenon may be ligand-mediated.

Efficient nanoparticle delivery is a major obstacle confronting cancer nanotechnology<sup>14, 16</sup>. In this context, we asked whether this mechanism (targeting tumour via a key monocyte subset) has a substantial effect on the total amount of SWNTs accumulating in tumour. We assessed the effect by computing the proportion of SWNTs in tumour contained within monocytes compared with the total amount of SWNTs in the tumour (which may arrive due to other targeting mechanisms such as extravasation, etc.<sup>7</sup>). The proportion of SWNT uptake into tumour due to monocyte uptake and infiltration depended on the peptide conjugated to SWNTs: nearly one quarter of RGD-SWNTs in the tumour on day 1 p.i. were due to this mechanism (Fig. 3c), which was significantly more than that in the plain or RAD-conjugated SWNT injected mice ( $p < 0.0001$  and  $p < 0.05$ , respectively) in which ~10–15% of SWNT uptake was due to monocyte delivery. Other, more conventional uptake mechanisms account for the remainder of SWNT uptake into tumour<sup>7</sup>. Possible sources of error, such as autofluorescence, are incorporated in the non-monocyte-driven uptake mechanisms, making our estimates of SWNT uptake due to monocytes a conservative lower bound.

## Conclusions

While the EPR effect enables SWNTs to reach the tumour<sup>7</sup>, here we demonstrate that SWNTs can also enter the tumour by uptake of cells circulating in the blood. This delivery mechanism can account for a considerable proportion (almost 25%) of SWNTs delivered to the tumour. The largest advantage afforded by this mechanism in oncology is that it is independent of the EPR effect and therefore of the enormous heterogeneity in extravasation that exists across different tumour types, particularly in humans; a common recent theme in the literature is the heterogeneity of the EPR effect in human cancers, including uncertainty in the degree of its effect in clinical cases<sup>8, 17</sup>. A Trojan Horse mechanism in which the nanoparticles are selectively delivered to tumour via circulating blood cells is likely much more reliable for all solid tumours and may thus be more translatable to human disease for both diagnostic and therapeutic efficacy. A second advantage arises from the fact that hypoxic and necrotic tumour regions, rendered inaccessible to nanoparticles delivered via typical targeting mechanisms via the vascular system<sup>18, 19</sup>, can now be reached with this mechanism; Ly-6C<sup>hi</sup> monocytes and the tumour-associated macrophages (TAMs) into which they differentiate are attracted to therapeutically critical hypoxic/necrotic tumour regions<sup>20</sup>, which could enable access of SWNTs to resistant tumour cells. A third advantage of this mechanism is that the nanoparticles are not limited by circulation time for uptake into tumour, but only by the circulation time of the immune cells taking them up in the blood, enabling the nanoparticles to be delivered continuously to tumour over a period of days. Additionally, it is important to note that while nanoparticles delivered to tumour generally

have been assumed to be free to bind directly to tumour cells, here we find that a considerable proportion are sequestered in monocytes/macrophages and thus presumably unable to attach to the tumour cell surface unless they are eventually released. We further note here that in contrast to conventional targeting assumptions, nanoparticles taken up into tumour via this targeting mechanism are independent of the EPR effect and thus independent of critical EPR concerns about how nanoparticle properties (e.g., nanoparticle size, shape, and surface charge) may affect EPR. These properties may affect nanoparticles' ability to enter monocytes, so future work will be required to determine if other types of nanoparticles, such as quantum dots and iron oxide nanoparticles amongst others<sup>14, 21</sup>, can be delivered into tumour beds similar to the mechanism we report here.

While the Trojan Horse mechanism described above may be highly advantageous for delivery, it relies on innate homing of monocytes alone. Our data suggest that RGD on the SWNT surface amplifies monocyte deposition in tumour (Fig. 3b), increasing the amount of SWNTs delivered (Fig. 3c) both in absolute numbers and as a proportion of total SWNT accumulation. This increased infiltration may be due to interactions between RGD and the vascular endothelial surface (Supplementary Fig. S4, discussed in Supplementary Information). Depending on peptide, between ~10–25% of total SWNTs found in the tumour were conservatively estimated to be due to monocyte uptake, making it a major targeting component. Indeed, this mechanism of uptake and tumour homing is likely partially responsible for SWNTs being one of the best known tumour targeting agents, with uptake of 10–15% ID/g<sup>5</sup>. Perhaps this is because monocytes allow continued accumulation of SWNTs: monocytes loaded with SWNTs continue to accumulate in tumour interstitium up to 7–9 days p.i. based on intravital microscopy (Fig. 3b) and the trends observed in Raman imaging of intrinsic SWNT signal (Supplementary Fig. S5). The ability to increase the uptake of monocytes in tumours ultimately might be exploited to improve immune-mediated cancer therapy using a variety of therapeutic strategies<sup>18, 22</sup>, potentially including induction of monocytes to become tumouricidal. In future applications, monocytes could be reprogrammed by nanoparticles<sup>23–26</sup> to help destroy or image tumours<sup>24</sup>. For example, because CD40-activated macrophages are tumouricidal<sup>27</sup> and Ly-6C<sup>hi</sup> monocytes differentiate into macrophages within tumours<sup>28</sup>, SWNTs might be equipped with activating molecules to provide a superior<sup>29</sup> nanoparticle-based activation trigger and RGD could be used to increase the number of macrophages to enhance tumour destruction.

Direct, selective delivery of nanoparticles and drugs into circulating immune cells has been a long-sought goal in medicine for wide-ranging applications<sup>12, 18, 30</sup>. Yet highly selective uptake has proven extremely challenging even in optimized *in vitro/ex vivo* conditions<sup>30–33</sup>, with most strategies displaying somewhat promiscuous uptake across several immune cell types. Ly-6C<sup>hi</sup> monocytes represent a premier cell group for increasing nanoparticle delivery to disease sites in general and toward novel routes for imaging and therapeutic interventions. This is because their native phenotype enables them to selectively infiltrate affected tissues in many diseases, such as to cancer via a Trojan Horse mechanism. Ly-6C<sup>hi</sup> monocytes are phenotypically, functionally, and physically (e.g., size, morphology) distinct from other monocyte subsets, including the other monocyte subset present in blood, Ly-6C<sup>low</sup> monocytes<sup>34, 35</sup>. Furthermore, Ly-6C<sup>hi</sup> monocytes account for only 2–5% of all circulating

white blood cells<sup>35, 36</sup>. Targeting this monocyte subset may be particularly important in cancer applications because Ly-6C<sup>hi</sup> monocytes differentiate into TAMs<sup>28</sup>, which form a critical component of the tumour stroma. In particular, TAMs have been implicated in the pathogenesis of cancer, requiring new strategies that selective SWNT targeting could potentially help provide. Because it is difficult for injected particles to reach often inaccessible TAMs deep in tumour hypoxic regions<sup>18, 37</sup>, targeting Ly-6C<sup>hi</sup> monocytes in blood could avoid this critical limitation. Our SWNTs enter the monocytes in blood, monocytes then undergo diapedesis into the tumour interstitium, become TAMs, and the TAMs could carry them to hypoxic regions. Moreover, our approach involves direct intravenous injection, thereby avoiding the need for *ex vivo* labeling of the cells<sup>18</sup> (though notably the *ex vivo* labeling method remains an option to further increase the amount of SWNTs delivered to the tumour). Last, with respect to eventual human clinical translation, we note that murine Ly-6C<sup>hi</sup> monocytes display high genetic homology and functionality to an analogous subset of monocytes in humans<sup>34</sup>, the CD14<sup>hi</sup>CD16<sup>-</sup> subset<sup>38</sup>.

We do not yet understand the mechanism for the selectivity of our SWNTs to Ly-6C<sup>hi</sup> monocytes. We also do not fully understand the mechanism of increased monocyte targeting to tumour via RGD, although imaging data indicates it is likely due to interaction between RGD and tumour vascular endothelium. Other limitations of our study include concerns about SWNT toxicity; however, we note that the excellent selectivity suggests that likely the main cell type of concern is Ly-6C<sup>hi</sup> monocytes (though it is possible inflammation or other effects could arise indirectly via the monocytes through released cytokines, antigen presentation, etc.). Unlike other studies that have shown deleterious effects of nanotubes (e.g., multi-walled, non-functionalized nanotubes<sup>39</sup>) on monocytes, our single-walled, biocompatible nanotubes do not activate monocytes 6h p.i. (Supplementary Fig. S3), indicating that SWNTs do not exert major effects on the monocytes based on surface marker analysis. Not only do SWNTs appear to be non-toxic to monocytes and mice in general<sup>40</sup>, but they can be protective/therapeutic to tissues as sensitive as the brain<sup>41</sup>. Nevertheless, we are working to understand the mechanism and effects of SWNTs on monocytes in greater detail.

In conclusion, we have identified a novel, key mechanism for nanoparticle uptake into tumours that accounts for a considerable proportion of the total uptake into tumours. Importantly, we have demonstrated that SWNTs target a key monocyte subset in the blood with exquisite selectivity and that RGD ligands attached to SWNTs can help increase the delivery of these cells into tumour sites, effectively “programming” them to enter tumour interstitium. This work may have important implications for cancer applications of nanoparticles such as the detection and treatment of cancer in the clinic; it highlights the value of circulating monocytes for targeted delivery by exploiting the fact that monocytes can easily enter and travel throughout tumours, has further implications for accurate pre-clinical identification of Ly-6C<sup>hi</sup> monocytes for disease and biological studies, and may ultimately have potential for diverse diseases such as atherosclerosis and arthritis in which this monocyte subset is directly implicated.

## Methods

### Nanoparticles

Peptide- and dye-conjugated SWNT bioconjugates were prepared as previously reported<sup>8, 42</sup> with slight modifications as follows. Raw Hipco SWNTs (Lot#R0513, Unidym, Sunnyvale, CA; diameter 0.8–1.2 nm) were placed in an aqueous solution of DSPE-PEG<sub>5000</sub>-Amine (NOF Corp) and sonicated for 1h, then centrifuged at 24,000 g for 6h to obtain short, PEGylated SWNTs in supernatant (100–300 nm in length<sup>40</sup>). SWNTs were filtrated using 100 kDa filters (Millipore) to remove excess coating polymer. For conjugation of both RGD (arginine-glycine-aspartic acid) (or control RAD (arginine-alanine-aspartic acid)) and Cy5.5 to SWNTs, Cy5.5-NHS (Invitrogen) and sulfo-SMCC (sulfosuccinimidyl 4-N-maleimidomethyl cyclohexane-1-carboxylate) (Pierce) were mixed at 1:5 molar ratios (0.2 mM : 1 mM) and incubated with the SWNT solution at pH 7.4 for 2h. Excess dye was removed via centrifugal filtration, and the SWNT solution was split into two halves and reacted overnight with 0.2 mM of thiolated RGD or RAD in the presence of 10 mM Tris(2-carboxyethyl) phosphine hydrochloride (TCEP, Sigma-Aldrich) at pH 7.4, yielding SWNT-PEG-Cy5.5-RGD and SWNT-PEG-Cy5.5-RAD with both Cy5.5 and RGD (RAD) conjugated on the SWNTs. Last, excess peptides were removed by filtrations using 100 kDa filters and then washed away by distilled water.

SWNT concentrations were determined spectrophotometrically (using a DU 640 from Beckman Coulter, Fullerton, CA) with an extinction coefficient of  $7.9 \times 10^6 \text{ M}^{-1} \cdot \text{cm}^{-1}$  at 808 nm as described previously. They were further analyzed for Cy5.5 content (~20 Cy5.5 dyes per SWNT). The surface charge of SWNTs was analyzed using a ZetaSizer Nano ZS (Malvern Instruments, Worcestershire, U.K.)<sup>8</sup>. PEG and Cy5.5 were verified to be on the SWNT surface (Supplementary Figs. S6–7).

### Intravital Microscopy

Male retired breeder SCID mice (n=30) both bearing dorsal windows (see Supplementary Methods for details on window implantation and the tumour model) and without dorsal windows were used for this study (mice without dorsal windows were employed for harvesting blood). To perform intravital microscopy, mice were anesthetized with isoflurane and placed onto a heated plate below the objective of an IV-100 intravital microscope (Olympus, Center Valley, PA). The mice were stabilized using a stainless steel customized stage by locking the titanium dorsal chamber into place (Supplementary Fig. S1). Angiosense 750 (a long-circulating dye; Perkin-Elmer, Waltham, MA) was injected to visualize the vasculature. 180  $\mu\text{l}$  of 0.068 mg/ml SWNTs (RGD-SWNTs, RAD-SWNTs, or plain SWNTs) were injected into each mouse 8–10 days after tumour inoculation. Mice were imaged during injection and for the following 4 hours. They were re-imaged at 6–8, 12, and 24 hours, then every day for a week following injection, and again on day 9 post-injection. Mice were imaged using the 488, 633, and 748 nm lasers and three appropriate output channels (green, red, and near-infrared filter sets). Output channels were scanned sequentially to prevent filter bleed-through. The presence of cells within vasculature was analyzed by reference to cell-shaped and sized objects (within the red, or Cy5.5, channel) within Angiosense-marked blood vessels and via associated FACS analyses of the blood.

The presence of monocytes containing SWNTs within the tumour (yet outside of the blood vessels) was also analyzed by reference to cell-shaped and sized objects within the Cy5.5 channel. All animal procedures were approved by the Stanford University Institutional Animal Care and Use Committee.

### Fluorescence Activated Cell Sorting (FACS) and Flow Cytometry

Mouse blood was drawn sub-mandibularly or from the tail vein into heparin-containing PBS solution at 2h and 6h post-intravenous injection of SWNTs. Sample processing and antibody staining details can be found in the Supplementary Methods. Cells were analyzed on Stanford FACS facility instruments (Becton Dickinson LSRII)<sup>43</sup>. Data were collected for  $\sim 0.2 \times 10^6$  cells. When sorting was required, SWNT-laden cells were isolated from the blood using FACS and analyzed (Becton Dickinson, FACS Aria II). Data were analyzed with FlowJo software (TreeStar).

### Dark-Field and Hyperspectral Imaging

After isolating cells loaded with SWNTs using FACS, we analyzed these cells using a BX-51 Olympus microscope (Olympus, Center Valley, PA) equipped with CytoViva® (Auburn, AL) enhanced darkfield illumination optics, using a 100X oil and variable 0.6–1.35 NA objective with full spectrum aluminum halogen source illumination. We obtained spectral image files from 400nm–1,000nm at 2nm spectral resolution using the CytoViva® hyperspectral imaging module. CytoViva® hyperspectral image analysis software was utilized to quantify the spectral response of SWNTs and to map them within the monocytes. A plain Cy5.5-SWNT solution (TEM, Supplementary Fig. S8) was applied as the standard to map SWNT presence and location within extracted living monocytes with hyperspectral imaging.

### Statistics

We quantified the peptide dependence (conjugated to SWNTs) of monocyte interactions with tumour blood vessels and the peptide- and time-dependence of monocyte trafficking into tumour and performed statistics. All statistical analyses were performed with Stata Release 9.2 (StataCorp LP, College Station, TX). A significance level of 0.05 was used. In particular, two-tailed student's t-tests were employed to test the peptide- and time-dependence of monocyte uptake into tumour.

### Supplementary Material

Refer to Web version on PubMed Central for supplementary material.

### Acknowledgments

This work was supported by the following grants: B.R.S. was supported by an NIH 25T post-doctoral training grant and currently by a K99/R00 award (K99 CA160764). S.S.G. was supported by a CCNE-T grant (NCI U54 CA119367) and ICMIC grant (P50 CA114747). We thank Catherine Ball for discussions related to this work. We gratefully acknowledge technical assistance in experiments and analysis from Megan Philips, Scott Tabakman, Jarrett Rosenberg, Sophie Kusy, Carsten Nielsen, Hongjie Dai, Ai Leen Koh, Robert Sinclair, Cristina Zavaleta, Jim Strommer, and CytoViva.

## References

1. Maeda H. The link between infection and cancer: Tumor vasculature, free radicals, and drug delivery to tumors via the EPR effect. *Cancer Sci.* 2013; 7:779–789. [PubMed: 23495730]
2. Hirsjarvi S, Passirani C, Benoit JP. Passive and active tumour targeting with nanocarriers. *Curr Drug Disc Technol.* 2011; 8:188–196.
3. Holgado MA, Martin-Banderas L, Alvarez-Fuentes J, Fernandez-Arevalo M, Arias JL. Drug targeting to cancer by nanoparticles surface functionalized with special biomolecules. *Curr Med Chem.* 2012; 19:3188–3195. [PubMed: 22612702]
4. Yu MK, Park J, Jon S. Targeting strategies for multifunctional nanoparticles in cancer imaging and therapy. *Theranostics.* 2012; 2:3–44. [PubMed: 22272217]
5. Liu Z, et al. In vivo biodistribution and highly efficient tumour targeting of carbon nanotubes in mice. *Nature Nanotech.* 2007; 2:47–52.
6. Hahn MA, Singh AK, Sharma P, Brown SC, Moudgil BM. Nanoparticles as contrast agents for in vivo bioimaging: current status and future perspectives. *Anal Bioanal Chem.* 2011; 399:3–27. [PubMed: 20924568]
7. Smith BR, et al. High-resolution, serial intravital microscopic imaging of nanoparticle delivery and targeting in a small animal tumor model. *Nano Today.* 2013; 8:126–137.
8. Smith BR, et al. Shape matters: intravital microscopy reveals surprising geometrical dependence for nanoparticles in tumor models of extravasation. *Nano Lett.* 2012; 12:3369–3377. [PubMed: 22650417]
9. Kam NW, Liu Z, Dai H. Carbon nanotubes as intracellular transporters for proteins and DNA: an investigation of the uptake mechanism and pathway. *Angew Chem.* 2006; 45:577–581. [PubMed: 16345107]
10. Lacerda L, et al. Translocation mechanisms of chemically functionalised carbon nanotubes across plasma membranes. *Biomaterials.* 2012; 33:3334–3343. [PubMed: 22289266]
11. Al-Jamal KT, et al. Cellular uptake mechanisms of functionalised multi-walled carbon nanotubes by 3D electron tomography imaging. *Nanoscale.* 2011; 3:2627–2635. [PubMed: 21603701]
12. Moghimi SM, et al. Particulate systems for targeting of macrophages: basic and therapeutic concepts. *J Innate Immun.* 2012; 4:509–528. [PubMed: 22722900]
13. Porter AE, et al. Direct imaging of single-walled carbon nanotubes in cells. *Nature Nanotechnol.* 2007; 2:713–717. [PubMed: 18654411]
14. Smith BR, et al. Real-time intravital imaging of RGD-quantum dot binding to luminal endothelium in mouse tumor neovasculature. *Nano Lett.* 2008; 8:2599–2606. [PubMed: 18386933]
15. Smith BR, Cheng Z, De A, Rosenberg J, Gambhir SS. Dynamic visualization of RGD-quantum dot binding to tumor neovasculature and extravasation in multiple living mouse models using intravital microscopy. *Small.* 2010; 6:2222–2229. [PubMed: 20862677]
16. Leimgruber A, et al. Behavior of endogenous tumor-associated macrophages assessed in vivo using a functionalized nanoparticle. *Neoplasia.* 2009; 11:459–468. [PubMed: 19412430]
17. Prabhakar U, et al. Challenges and Key Considerations of the Enhanced Permeability and Retention Effect for Nanomedicine Drug Delivery in Oncology. *Cancer Res.* 2013; 73:2412–2417. [PubMed: 23423979]
18. Choi MR, et al. A cellular Trojan Horse for delivery of therapeutic nanoparticles into tumors. *Nano Lett.* 2007; 7:3759–3765. [PubMed: 17979310]
19. Owen MR, et al. Mathematical modeling predicts synergistic antitumor effects of combining a macrophage-based, hypoxia-targeted gene therapy with chemotherapy. *Cancer Res.* 2011; 71:2826–2837. [PubMed: 21363914]
20. Murdoch C, Giannoudis A, Lewis CE. Mechanisms regulating the recruitment of macrophages into hypoxic areas of tumors and other ischemic tissues. *Blood.* 2004; 104:2224–2234. [PubMed: 15231578]
21. Smith BR, et al. Localization to atherosclerotic plaque and biodistribution of biochemically derivatized superparamagnetic iron oxide nanoparticles (SPIONs) contrast particles for magnetic resonance imaging (MRI). *Biomed Microdevices.* 2007; 9:719–727. [PubMed: 17562181]

22. Lacerda L, Raffa S, Prato M, Bianco A, Kostarelos K. Cell-penetrating CNTs for delivery of therapeutics. *Nano Today*. 2007; 2:38–43.
23. Yeste A, Nadeau M, Burns EJ, Weiner HL, Quintana FJ. Nanoparticle-mediated codelivery of myelin antigen and a tolerogenic small molecule suppresses experimental autoimmune encephalomyelitis. *Proc Natl Acad Sci USA*. 2012; 109:11270–11275. [PubMed: 22745170]
24. Cubillos-Ruiz JR, et al. Polyethylenimine-based siRNA nanocomplexes reprogram tumor-associated dendritic cells via TLR5 to elicit therapeutic antitumor immunity. *J Clin Invest*. 2009; 119:2231–2244. [PubMed: 19620771]
25. Leuschner F, et al. Therapeutic siRNA silencing in inflammatory monocytes in mice. *Nature Biotechnol*. 2011; 29:1005–1010. [PubMed: 21983520]
26. Roy A, Singh MS, Upadhyay P, Bhaskar S. Combined Chemo-immunotherapy as a Prospective Strategy To Combat Cancer: A Nanoparticle Based Approach. *Mol Pharm*. 2010
27. Beatty GL, et al. CD40 agonists alter tumor stroma and show efficacy against pancreatic carcinoma in mice and humans. *Science*. 2011; 331:1612–1616. [PubMed: 21436454]
28. Movahedi K, et al. Different tumor microenvironments contain functionally distinct subsets of macrophages derived from Ly6C(high) monocytes. *Cancer Res*. 2010; 70:5728–5739. [PubMed: 20570887]
29. Gu L, et al. Multivalent porous silicon nanoparticles enhance the immune activation potency of agonistic CD40 antibody. *Adv Mater*. 2012; 24:3981–3987. [PubMed: 22689074]
30. Elamanchili P, Diwan M, Cao M, Samuel J. Characterization of poly(D,L-lactic-co-glycolic acid) based nanoparticulate system for enhanced delivery of antigens to dendritic cells. *Vaccine*. 2004; 22:2406–2412. [PubMed: 15193402]
31. Cruz LJ, et al. Targeting nanosystems to human DCs via Fc receptor as an effective strategy to deliver antigen for immunotherapy. *Mol Pharm*. 2011; 8:104–116. [PubMed: 21121669]
32. Cruz LJ, et al. Multimodal imaging of nanovaccine carriers targeted to human dendritic cells. *Mol Pharm*. 2011; 8:520–531. [PubMed: 21381651]
33. Gunn J, et al. A multimodal targeting nanoparticle for selectively labeling T cells. *Small*. 2008; 4:712–715. [PubMed: 18528851]
34. Saha P, Geissmann F. Toward a functional characterization of blood monocytes. *Immunol Cell Biol*. 2011; 89:2–4. [PubMed: 21102535]
35. Yona S, Jung S. Monocytes: subsets, origins, fates and functions. *Curr Opin Hematol*. 2010; 17:53–59. [PubMed: 19770654]
36. Shi C, Pamer EG. Monocyte recruitment during infection and inflammation. *Nat Rev Immunol*. 2011; 11:762–774. [PubMed: 21984070]
37. Primeau AJ, Rendon A, Hedley D, Lilge L, Tannock IF. The distribution of the anticancer drug Doxorubicin in relation to blood vessels in solid tumors. *Clin Cancer Res*. 2005; 11:8782–8788. [PubMed: 16361566]
38. Ingersoll MA, et al. Comparison of gene expression profiles between human and mouse monocyte subsets. *Blood*. 2010; 115:e10–19. [PubMed: 19965649]
39. De Nicola M, et al. Effects of carbon nanotubes on human monocytes. *Ann N Y Acad Sci*. 2009; 1171:600–605. [PubMed: 19723110]
40. Schipper ML, et al. A pilot toxicology study of single-walled carbon nanotubes in a small sample of mice. *Nature Nanotech*. 2008; 3:216–221.
41. Lee HJ, et al. Amine-modified single-walled carbon nanotubes protect neurons from injury in a rat stroke model. *Nature Nanotech*. 2011; 6:121–125.
42. Liu Z, Tabakman SM, Chen Z, Dai H. Preparation of carbon nanotube bioconjugates for biomedical applications. *Nature Prot*. 2009; 4:1372–1382.
43. Herzenberg LA, Tung J, Moore WA, Parks DR. Interpreting flow cytometry data: a guide for the perplexed. *Nat Immunol*. 2006; 7:681–685. [PubMed: 16785881]
44. Ghosn EE, et al. Two physically, functionally, and developmentally distinct peritoneal macrophage subsets. *Proc Natl Acad Sci USA*. 2010; 107:2568–2573. [PubMed: 20133793]

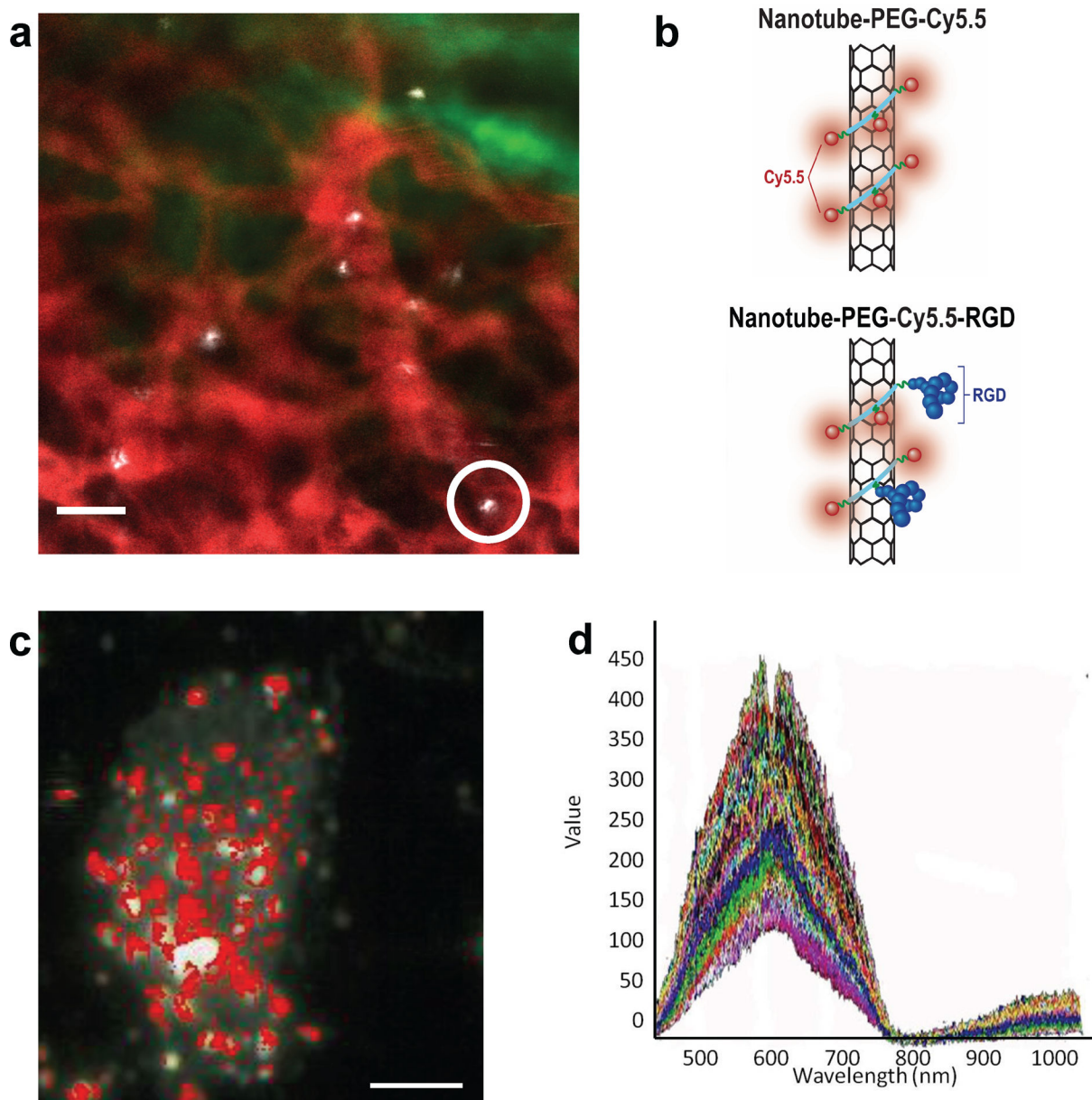


**Figure 1. SWNT uptake into circulating cells**

**a.** Representative intravital fluorescence image of single-walled carbon nanotube (SWNT)-laden circulating cells in tumour vasculature (one example cell is circled). Grayscale – SWNT-Cy5.5; Red – long-circulating dye highlighting tumour blood vessels; Green – EGFP (enhanced green fluorescent protein)-transfected tumour cells. Scale-bar: 40  $\mu\text{m}$ . **b.** Schematic of SWNTs non-covalently coated with a block amphiphile phospholipid PEG on the surface, with hydrophobic segment (light blue) associated with the SWNT surface and the hydrophilic segment (green) attached to Cy5.5 fluorescent dye (red sphere) and/or RGD (or RAD) peptide (blue cyclic ball structure). SWNTs were injected into SCID mice with implanted window chambers and imaged dynamically over weeks. **c.** Darkfield image of SWNTs in a live circulating blood cell extracted from a mouse and FACS-sorted for positive SWNT-Cy5.5 signal (SWNTs pseudocolored in red, analyzed by hyperspectral imaging).

Scale bar: 1  $\mu\text{m}$ . **d.** The hyperspectral spectra are taken from a plain SWNT-cy5.5 solution in PBS. Each curve represents scattered photons from a pixel in the SWNT solution. The y-axis is in dimensionless units, a digital number representing a conversion from the camera voltage to a digital quantity. SWNTs are pseudocolored red in (c) based on the spatial localization of this reference SWNT hyperspectral spectrum overlaid on the darkfield image. This analysis confirms the presence of SWNTs in circulating blood cells.

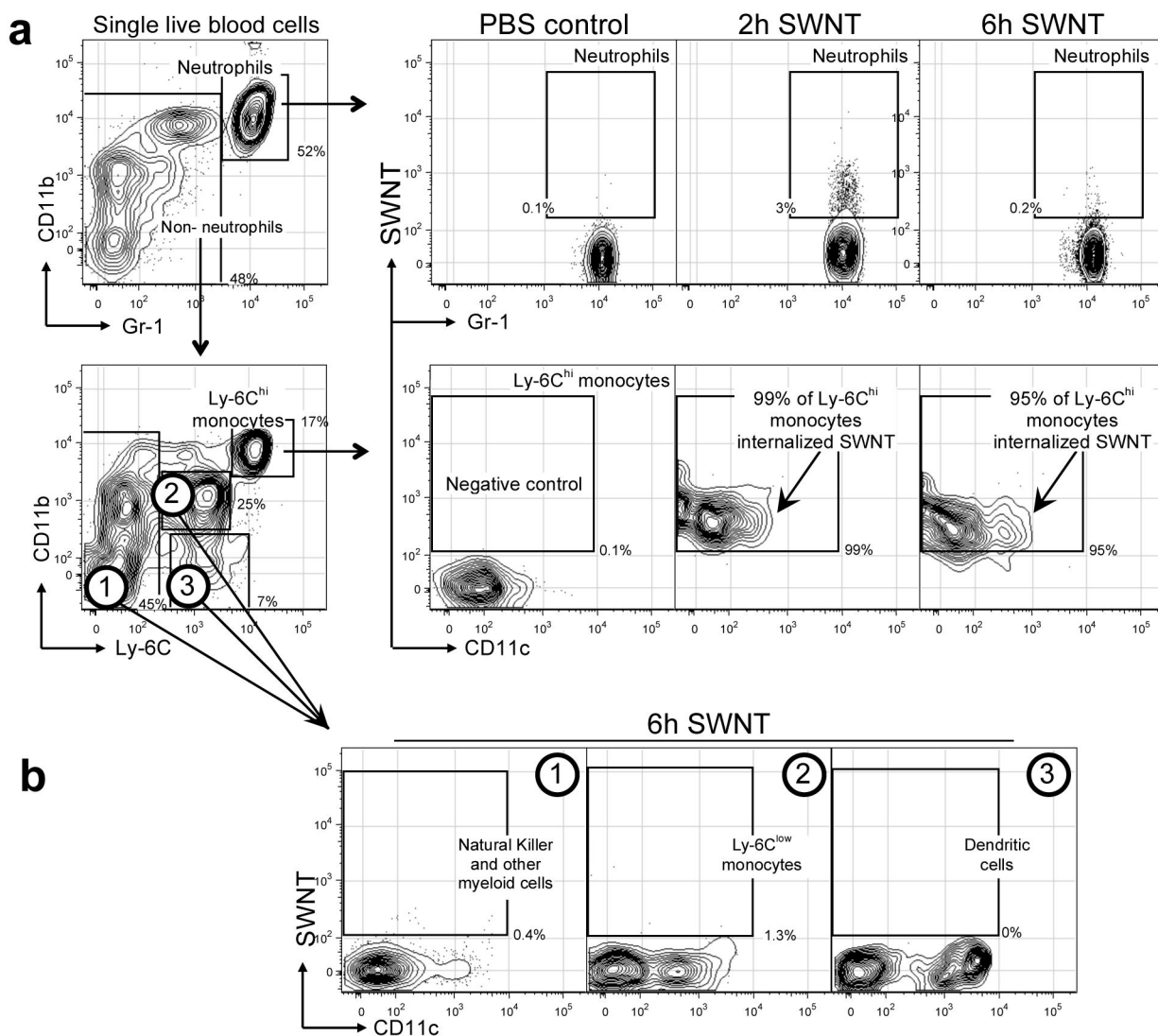


**Figure 2. Flow cytometry plots showing selective uptake of SWNTs into a blood monocyte subset**  
**a.** Blood was harvested 2 hours and 6 hours after injection of plain SWNT-Cy5.5 and stained with specific antibodies for flow cytometry analysis. Here contour plots are used to represent cell numbers graphically. The upper left plot represents total single live white blood cells analyzed for their surface expression levels of CD11b and Gr-1 (a marker which identifies granulocytes and is highly expressed on neutrophils). The cells expressing higher levels (fluorescence intensity) of surface CD11b and Gr-1 are known to be neutrophils, which represent 52% of total cells in blood (upper right cluster of cells gated as neutrophils; the proportion of neutrophils taking up SWNTs is displayed in plots along the top right row). Non-neutrophils are gated in the lower left of the plot. The cells expressing higher levels of Ly-6C and CD11b (among the non-neutrophil cells), gated in the upper right of the bottom left plot, represent Ly-6C<sup>hi</sup> monocytes (inflammatory monocytes). Plots in the second row demonstrate the selectivity of SWNT uptake into Ly-6C<sup>hi</sup> monocytes (nearly 100% of blood monocytes take up SWNTs at 2 hours, middle right plot). Less than 3% of cells in other subpopulations in blood take up SWNTs, including neutrophils. **b.** At 6 hours

p.i. other cell types in the blood still do not take up SWNTs. The cells contained in each plot are derived from the gates drawn on part (a) of the figure and labeled “1”, “2”, and “3”. These plots consist of the remaining blood cells after neutrophils and Ly-6c<sup>hi</sup> monocytes were removed from the analysis. These cell populations, including Natural Killer cells, Ly-6C<sup>low</sup> monocytes, and dendritic cells (CD11c+ populations), do not take up SWNTs. Flow cytometry plot data is representative of n=5 mice per group. Numbers near the gates represent the percentage of cells in the plot that are present within the drawn gate. Gates are drawn based on fluorescence minus one negative controls<sup>44</sup>.

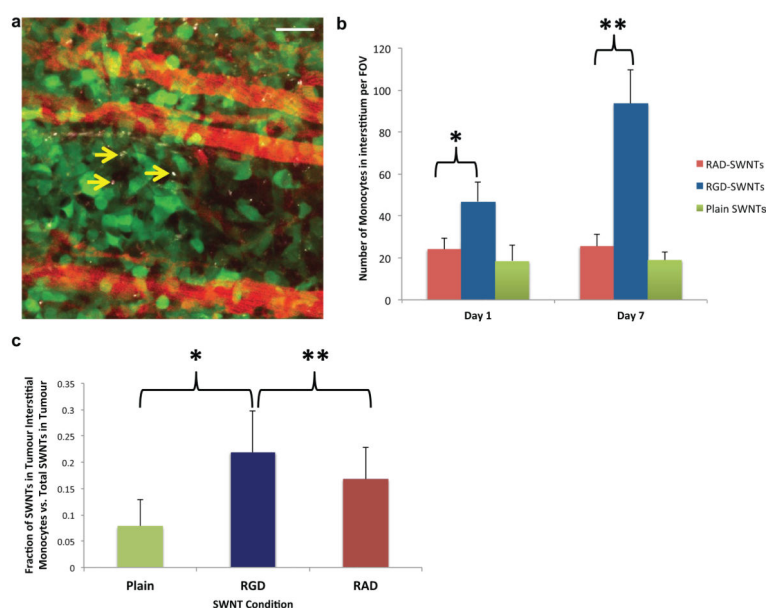


**Figure 3. SWNT-laden monocytes enter the tumour interstitium in a peptide-dependent manner**  
**a.** A representative intravital micrograph of a tumour region (tumour cells, green; blood vessels, red; SWNTs, grayscale). Yellow arrows point to several SWNT-laden monocytes within the tumour interstitium. Scale bar: 50  $\mu$ m. **b.** Bar graph shows that significantly more monocytes carrying RGD-SWNTs accumulate in tumour interstitium than in the RAD-SWNT and plain SWNT conditions on days 1 and 7 post-injection of SWNTs. Moreover, significantly more RGD-SWNT laden monocytes are in the interstitium per FOV on day 7 than on day 1 ( $p < 0.001$ ). \*  $p < 0.05$ ; \*\*  $p < 0.0005$ . Error bars S.E.M. FOV, Field of view. **c.** SWNTs can enter tumour through a variety of mechanisms, such as leakage through blood vessel pores. This graph shows the relative amount of SWNTs in the tumour interstitium that were ferried in via the “Trojan Horse” monocytes compared to all SWNTs within tumour interstitium as a function of peptide on Day 1 p.i. More than 20% of SWNTs in the tumour interstitium in the RGD-SWNT condition are carried in via monocytes. \*  $p < 0.0001$ ; \*\*  $p < 0.025$ . Error bars S.D.